Design Optimization Tool for Synthetic Jet Actuators Using Lumped Element Modeling

Final Report for NAG-1-03031

April 8, 2003 – April 7, 2005

Attention: Susan Gorton
NASA Langley Research Center
Hampton, VA 23681-2199
Phone: (757) 864-5059
FAX : (757) 864-7897
email: S.A.GORTON@LaRC.NASA.GOV

Prepared by:

Quentin Gallas, Mark Sheplak and Louis N. Cattafesta III
Department of Mechanical and Aerospace Engineering,
University of Florida
P. O. Box 116250
Gainesville, FL 32611-6250
Email: cattafes@ufl.edu
Phone: (352) 846-3017
Fax: (352) 392-7303

Table of Contents

Summary

The performance specifications of any actuator are quantified in terms of an exhaustive list of parameters such as bandwidth, output control authority, etc. Flow-control applications benefit from a known actuator frequency response function that relates the input voltage to the output property of interest (e.g., maximum velocity, volumetric flow rate, momentum flux, etc.). Clearly, the required performance metrics are application specific, and methods are needed to achieve the optimal design of these devices. Design and optimization studies have been conducted for piezoelectric cantilever-type flow control actuators, but the modeling issues are simpler compared to synthetic jets.[1] Here, lumped element modeling (LEM) is combined with equivalent circuit representations to estimate the nonlinear dynamic response of a synthetic jet as a function of device dimensions, material properties, and external flow conditions.[2,3] These models provide reasonable agreement between predicted and measured frequency response functions and thus are suitable for use as design tools. In this work, we have developed a Matlab-based design optimization tool for piezoelectric synthetic jet actuators based on the lumped element models mentioned above. Significant improvements were achieved by optimizing the piezoceramic diaphragm dimensions. Synthetic-jet actuators were fabricated and benchtop tested[3] to fully document their behavior and validate a companion optimization effort. It is hoped that the tool developed from this investigation will assist in the design and deployment of these actuators.

Optimization of Synthetic Jet Actuators

Problem Description

Synthetic or "zero-net mass flux" jets[4] are commonly used as flow-control actuators in a wide spectrum of applications including jet vectoring,[5] separation control,[6,7,8] and boundary layer control.[9,10] The performance specifications of any actuator are quantified in terms of an exhaustive list of parameters such as bandwidth, control authority, etc. Flow-control applications require a known actuator frequency response function that relates the input voltage to the output property of interest (e.g., maximum velocity, volumetric flow rate, momentum flux, etc.). Clearly, the required performance metrics are application specific, and methods are needed to achieve the optimal design of these devices. This work summarizes lumped element modeling (LEM) of synthetic jet actuator and presents results for the optimization of synthetic jet actuators based on LEM, namely the optimization of the cavity and orifice dimensions and the piezoelectric composite diaphragm.

Objectives

The objectives of this report are:

- To summarize the use of lumped element modeling as a design tool for the optimization of synthetic jet actuators
- To optimize the cavity and orifice dimensions of the actuator for a given piezoelectric diaphragm
- To optimize unimorph and bimorph piezoelectric diaphragm for various configurations
- To develop a Matlab-based optimal design synthesis tool

Approach

We have investigated various actuators for active flow-control: oscillating flaps and synthetic-jet actuators. In addition, lumped element modeling has been successfully applied to piezoelectric-driven synthetic jet actuators as a design tool.[2] In this research, synthetic jet actuators are modeled and optimized based on lumped element modeling.[11,12,13]

Lumped Element Modeling

A cross-sectional schematic and corresponding equivalent circuit representation for a typical piezoelectric-driven synthetic jet are shown in Figure 1, using LEM. The details of the circuit parameter estimation techniques, assumptions, and limitations are given by Gallas et al.[2] The structure of the equivalent circuit is explained as follows. A harmonic voltage V_{ac} is applied across the piezoceramic to create an effective acoustic pressure that drives the diaphragm into motion. This represents a conversion from electrical energy to acoustic energy and is represented by an ideal transformer possessing a turns ratio ϕ_a. The motion of the diaphragm (i.e., volume velocity, Q) can store potential energy via compressibility effects in the cavity (Q_c) and/or can store kinetic energy via oscillatory flow through the orifice (Q_{out}). Physically, this is represented as a volume velocity divider, $Q = Q_c + Q_{out}$.

There are several simplifying assumptions employed in the current model. First, the synthetic jet is assumed to exhaust into a semi-infinite quiescent air medium. In practice, these devices interact with a boundary layer that greatly alters the jet-exit velocity profile and thus the total orifice impedance.[15] The corresponding differences in the frequency response functions of a synthetic jet actuator exhausting into a quiescent medium versus one exhausting into a boundary layer means that the bench-top calibration of these devices is insufficient to accurately

estimate the volume velocity or momentum flux exhausted into a cross flow for a given excitation voltage. Second, compressibility effects in the orifice, but not in the cavity, are neglected. The incorporation of these effects into the lumped element model is an ongoing research area in the engine nacelle acoustic liner community.[16] We have completed some extensions of the lumped element modeling technique to handle a grazing boundary layer. The details are beyond the scope of this report, but the interested reader is referred to Gallas et al.[17,18,3]

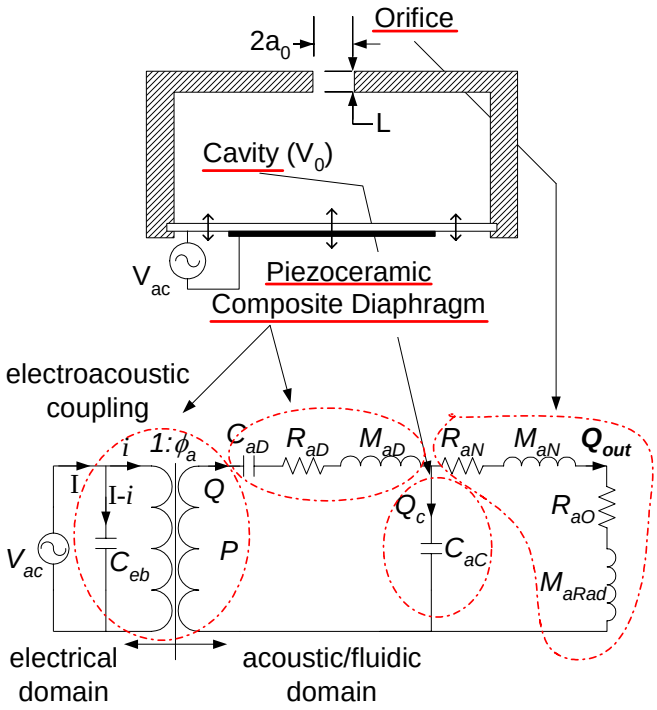

Figure 1: Schematic representation and equivalent circuit model of a piezoelectric-driven synthetic jet.

The frequency response function of the volume flow rate through the orifice per applied voltage for the equivalent circuit shown in Figure 1 is a four-pole, single-zero dynamic system,[2]

$$\frac{Q_{out}(s)}{V_{ac}(s)} = \frac{d_a s}{a_4 s^4 + a_3 s^3 + a_2 s^2 + a_1 s + 1}, \qquad \{1\}$$

where

$$
\begin{aligned}
a_1 &= C_{aD}\left(R_{aO}+R_{aN}+R_{aD}\right)+C_{aC}\left(R_{aO}+R_{aN}\right),\\
a_2 &= C_{aD}\left(M_{aRad}+M_{aN}+M_{aD}\right)+C_{aC}\left(M_{aRad}+M_{aN}\right)+C_{aC}C_{aD}R_{aD}\left(R_{aO}+R_{aN}\right),\\
a_3 &= C_{aC}C_{aD}\left[M_{aD}\left(R_{aO}+R_{aN}\right)+\left(M_{aRad}+M_{aN}\right)R_{aD}\right], \text{ and}\\
a_4 &= C_{aC}C_{aD}M_{aD}\left(M_{aRad}+M_{aN}\right).
\end{aligned}
\qquad \{2\}
$$

To first order, the coefficients in Eq. {2} are constants determined via simple algebraic expressions as a function of geometry and material properties. This model includes one empirical constant, R_{aD}, that represents the structural damping of the piezoelectric composite. In general, some of the coefficients exhibit frequency and amplitude dependence (i.e., due to nonlinear effects). Specifically, R_{aO} is a non-linear orifice resistance that is proportional to the volume velocity, $Q_{out}(s)$.

For a dc voltage ($s=0$), the volume velocity is zero. At low frequencies ($s\to 0$), the volume velocity is proportional to $j\omega d_a V_{ac}$. At high frequencies ($s\to\infty$),

$$
\frac{Q_{out}}{V_{ac}} \cong \frac{d_a}{C_{aC}C_{aD}M_{aD}\left(M_{aN}+M_{aRad}\right)s^3}, \qquad \{3\}
$$

and the output attenuates at 60 dB/decade.

The four-pole system in Eq. {1} possesses two resonant frequencies, f_1 and $f_2 > f_1$, that are related to the short-circuit piezoelectric diaphragm natural frequency f_D,

$$
f_D = \frac{1}{2\pi}\sqrt{\frac{1}{M_{aD}C_{aD}}}, \qquad \{4\}
$$

and the Helmholtz resonator frequency f_H,

$$
f_H = \frac{1}{2\pi}\sqrt{\frac{1}{\left(M_{aN}+M_{aRad}\right)C_{aC}}}, \qquad \{5\}
$$

by the equality

$$f_1 f_2 = f_D f_H \,. \qquad \{6\}$$

From Eq. {6}, it is obvious that the cavity volume and the orifice dimensions, as well as the piezoelectric-diaphragm characteristics determine the dynamic response of the synthetic jet.

Gallas et al.[2] have experimentally validated the lumped element model for two different prototypical synthetic jet actuators using phase-locked Laser-Doppler Velocimetry. The amplitude of the piezoelectric excitation voltage was 25 V in all cases. The comparison between the full nonlinear model prediction and the experiments are shown in Figure 2 and Figure 3. In both figures, the centerline velocity magnitude is plotted as a function of frequency. For the lumped element model predictions, the centerline velocity was estimated by modeling the flow in the orifice as flow in a circular duct driven by an oscillatory pressure gradient. The first case (I, Figure 2) clearly illustrates the two resonant frequencies of the coupled oscillator. The second case (II, Figure 3) corresponds to a system possessing a single dominant peak. The lower peak at $f_1 \approx 315$ Hz is heavily damped in this case due to the frequency dependent nonlinear orifice resistance term R_{aO}. In both cases, there is sufficient agreement between prediction and experiment to justify the employment of LEM as a design and optimization tool. It is important to note that the underlying assumptions used to derive each lumped element limit the applicable frequency range of the corresponding element from dc to some upper limiting frequency (see, for example, Rossi[14]).

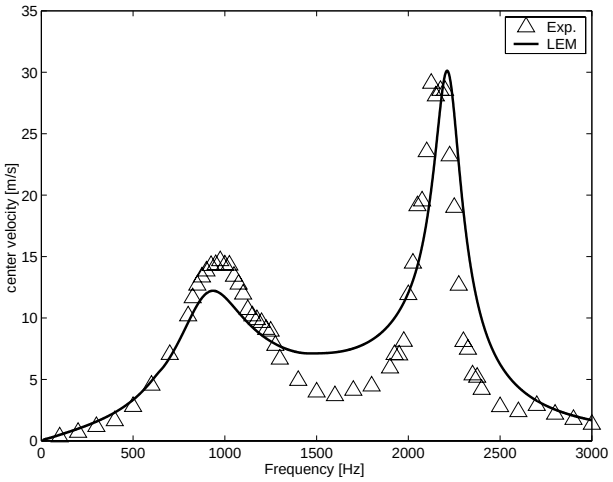

Figure 2: Comparison between the lumped element model and experiment for Case I.[2]

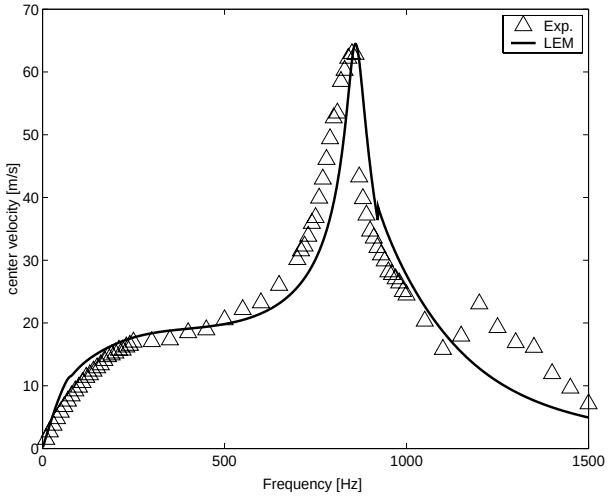

Figure 3: Comparison between the lumped element model and experiment for Case II.[2]

The lumped element model presented above is thus a powerful design tool that enables the multi-energy domain dynamic modeling of a synthetic jet actuator. This model is therefore used as a vehicle to enable optimization. The optimization problem is solved via MATLAB's optimization toolbox.

Cavity and Orifice Optimization

Details of the modeling procedure are presented in Gallas,[3] and optimization results are presented in Gallas et al.[11,13] First, a constrained optimization of the cavity volume and orifice

dimensions of the two baseline synthetic jets presented above, each with a given piezoelectric diaphragm, has been performed. The goal is to improve the performance of the nominal designs presented in Figure 2 (Case I) and Figure ***3*** (Case II). The objective function, constraints, and design variables are summarized in Table 1. Specifically, Case I is optimized using one cost function, while Case II is optimized using a different cost/objective function.

Table 1: Summary of optimization problem for a synthetic jet actuator.

Objective	**Constraints**	**Variables**
$\int_0^{f_{\lim}} u_0(f)\,df$ = integrated centerline velocity over a desired frequency range	• Upper/Lower bounds on variables: <u>Case I:</u> $\begin{cases} 0.125 \le a_0 \le 2 \\ 0.5 \le L \le 20 \\ 1152 \le V_0 \le 47,640 \end{cases}$ <u>Case II:</u> $\begin{cases} 0.125 \le a_0 \le 2 \\ 0.38 \le L \le 20 \\ 780 \le V_0 \le 21,270 \end{cases}$ • Orientation aspect ratio $L/a_0 \ge 1$ • Fixed input voltage V_{ac} = 25 V	a_0 [mm] L [mm] V_0 [mm^3]
$u_0(f_2)$ = centerline velocity at a fixed frequency f_2	• Upper/Lower bounds on variables: <u>Case II:</u> $\begin{cases} 0.125 \le a_0 \le 2 \\ 0.38 \le L \le 20 \\ 780 \le V_0 \le 21,270 \end{cases}$ • Natural frequency f_2 = 820 Hz • Orientation aspect ratio $L/a_0 \ge 1$ • Fixed input voltage V_{ac} = 25 V	a_0 [mm] L [mm] V_0 [mm^3]

The first cost function employed maximizes the integrated centerline velocity over the entire frequency range, $\int_0^{f_{\lim}} u_0(f)\,df$ where the upper limit of integration is 3000 Hz and 1500 Hz for Case I and II, respectively. The motivation for such an objective function is to increase

the broadband response of the actuator. The constraints on the orifice radius are motivated by device manufacturability and flow perturbation concerns, while the minimum orifice length constraint is driven by the requirement that the orifice plate be rigid. The volume range is dictated by size limitations. In addition, constraints are imposed on the orifice aspect ratio (since the current lumped element model is not valid for small L/a_0) and by fixing the piezoelectric drive voltage. ***Figure** 4* shows the resulting optimized frequency response function compared to the nominal response for Case I. The frequency response function increased over the entire frequency range by decreasing V_0, a_0, and L. In addition, the first resonant peak is heavily damped in the optimized response.

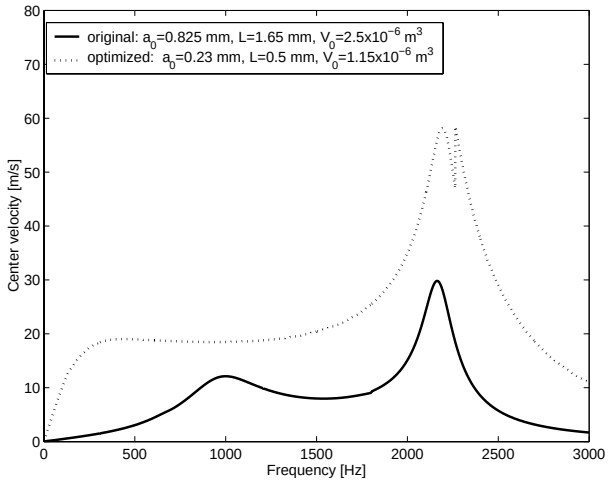

Figure 4: Optimization of Case I, maximizing the overall output.

The results using a similar approach for Case II are shown in ***Figure** 5*. Again, the frequency response function increased over nearly the entire frequency range by decreasing V_0, a_0, and L. In addition, the flat portion of the response function is increased and the second resonant peak is moved to a higher frequency. This actuator design is useful for applications that require a flat broadband response.

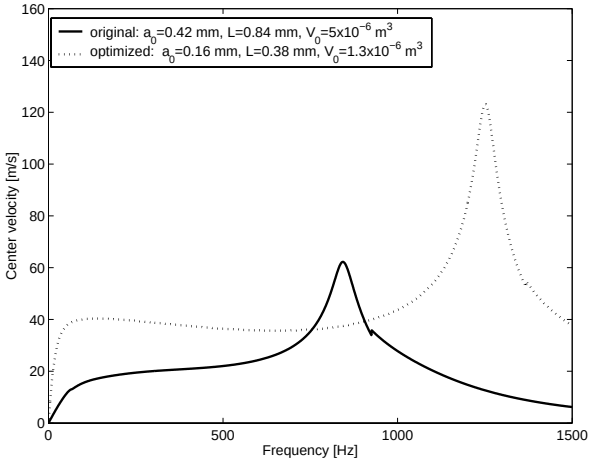

Figure 5: Optimization of Case II, maximizing the overall output.

The second cost function employed maximizes the centerline velocity at the second resonant frequency of the system, $u_0(f_2)$. From a practical standpoint, this optimization is useful for applications requiring high actuation authority over a narrow frequency range. The constraints on the orifice and cavity geometry, as well as the aspect ratio and drive voltage are similar to those outlined above. A new equality constraint, however, is placed on the location of the second resonant frequency. The results of this optimization for Case II are shown in ***Figure 6***. The second resonant peak is increased as desired (by ~ 35%). In addition, the broadband response, especially at the lower frequencies, is increased with respect to the nominal case.

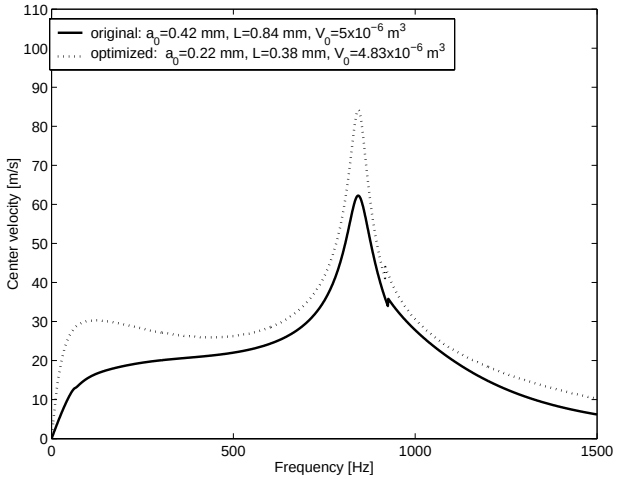

Figure 6: Optimization of Case II, maximizing the second peak.

While the optimization studies in this section indicate the promise of improved performance, additional gains can likely be achieved by optimizing the piezoelectric composite diaphragm.

Piezoelectric Diaphragm Optimization

The piezoelectric diaphragm optimization is described in this section. The configuration here is the standard unimorph inner-disc piezoceramic patch bonded to a metal shim. The basic modeling concepts of the piezoelectric diaphragm are explained as follows. Ideally, a piezoelectric actuator is a linear, conservative, reciprocal transducer.[14] The piezoelectric composite deforms in response to both an applied ac voltage and a differential pressure. The lumped piezoelectric coupling equations for the transduction model are[19]

$$\begin{Bmatrix} \Delta V \\ q \end{Bmatrix} = \begin{bmatrix} C_{aD} & d_a \\ d_a & C_{EF} \end{bmatrix} \begin{Bmatrix} P \\ V_{ac} \end{Bmatrix}, \qquad \{7\}$$

where ΔV is the volume displaced by the plate due to the application of a differential pressure P and/or voltage V_{ac}, q is the charge stored on the piezoelectric electrodes, C_{EF} is the electrical free capacitance of the piezoelectric material, C_{aD} is the short-circuit acoustic compliance of the plate, and d_a is the effective acoustic piezoelectric coefficient.

The acoustic mass M_{aD} is determined by equating the lumped kinetic energy of the vibrating diaphragm expressed in acoustic conjugate power variables to the total kinetic energy. The determination of the lumped element parameters for this two-port model requires the solution of the transverse static deflection field as a function of pressure and voltage loading. For this study, linear laminated plate theory is used to solve for the transverse static deflection, and an optimization scheme is then implemented using this two-port model. The details of the composite plate model are presented in Prasad et al.[19] The optimization objective function

maximizes the achievable displaced volume per applied voltage, $d_a = \Delta V\big|_{P=0} / V_{ac,\max}$, compared to the nominal values for Cases I and II. The optimization procedure (design variables, constraints, cost function, etc.) is described in Gallas et al.[11]. The results are presented in Table *2*. The optimum design slightly improves (by ~6%) the volume displacement achieved for the nominal Case I, while a 52% improvement is achieved compared to the nominal Case II.

Table 2: Optimization results of piezoelectric diaphragms with an inner-disc configuration.

Table 2: Optimization results of piezoelectric diaphragm configurations: Case I, R_3=11.5 mm, f_D=2114Hz. Max(Q). no minimum gauge for t_p and t_s			
	Original	Optimum Unimorph	Optimum Bimorph
R_3 *(mm)*	11.5	11.5	11.5
R_2 *(mm)*	Na	11.5	11.5
R_1 *(mm)*	10.00	11.39	11.31
t_s *(mm)/(mil)*	0.150 / 5.9	0.024 / 0.9	0.024 / 0.9
t_p *(mm)/(mil)*	0.08 / 3.1	0.243 / 9.6	0.135 / 5.3
f_D *(Hz)*	2114	2114	2114
$Q\ x10^{-10}\ (m^3)$	52.3	155.7	267.2
V_{max} *(V)*	95	288	159

Table 3: Optimization results of piezoelectric diaphragms with an inner-disc configuration.

Table 3: Optimization results of piezoelectric diaphragm configurations: Case II, R_3=18.5 mm, f_D=632Hz. Max(Q). no minimum gauge for t_p and t_s			
	Original	Optimum Unimorph	Optimum Bimorph
R_3 *(mm)*	18.5	18.5	18.5
R_2 *(mm)*	na	18.5	18.5
R_1 *(mm)*	12.50	18.32	18.32
t_s *(mm)/(mil)*	0.10/ 3.9	0.018 / 0.7	0.0062 / 0.2
t_p *(mm)/(mil)*	0.11 / 4.3	0.188 / 7.4	0.11 / 4.3
f_D *(Hz)*	632	632	632
$Q\ x10^{-10}\ (m^3)$	561	1348	2460
V_{max} *(V)*	130	222	130

Table 4: Material properties.

Property	Piezoceramic (PZT-5A)	Shim (Brass)
Elastic Modulus (Pa)	6.3×10^{10}	8.963×10^{10}
Poisson's Ratio	0.33	0.324
Density (kg/m^3)	7700	8700
Rel. Dielectric Constant	1750	-
d_{31} (m/V)	-1.75×10^{-10}	-

In addition, a study to find the optimal piezoelectric composite circular plate configuration and design for maximized volume displacement and bandwidth has been conducted. Their tradeoff and practical manufacturing requirements are considered via optimization techniques. The results for brass shim and PZT-5A (Table 3) combinations are summarized below.

❖ The analytical composite plate model has been verified for a generic design via a commercial FEA code (see ***Figure** 7*).

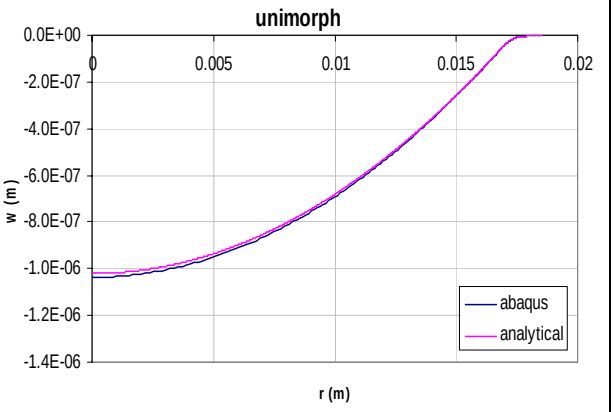

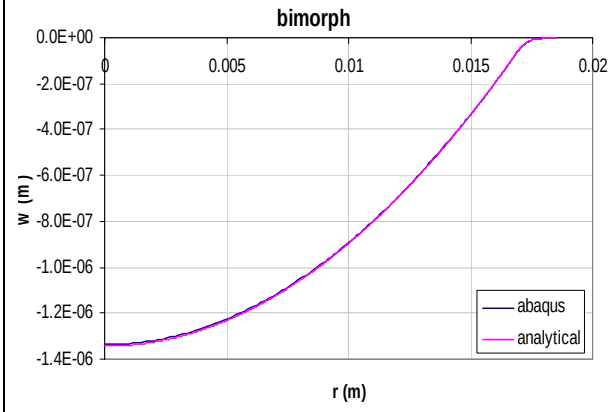

Design

R_1 (mm)	R_2 (mm)	R_3 (mm)	t_p (mm)	t_s (mm)
16.89	17.58	18.50	0.123	0.081

Figure 7: **Validation of analytical model via Abaqus FEM code. The vertical deflection per unit applied voltage is shown plotted vs. radius.**

❖ An optimization study has been conducted to determine the optimum geometry of various unimorph and bimorph configurations (Figure 8). The objective function chosen was to maximize the static (i.e., dc) volume displaced by the diaphragm, Q (at the maximum operational voltage of the device), subject to constraints on the minimum allowed natural frequency $\left(f_D \right)$ of the diaphragm and other geometric constraints. The resulting designs tended towards full coverage of the shim by the inner piezoceramic layer, that is $R_1, R_2 \to R_3$.

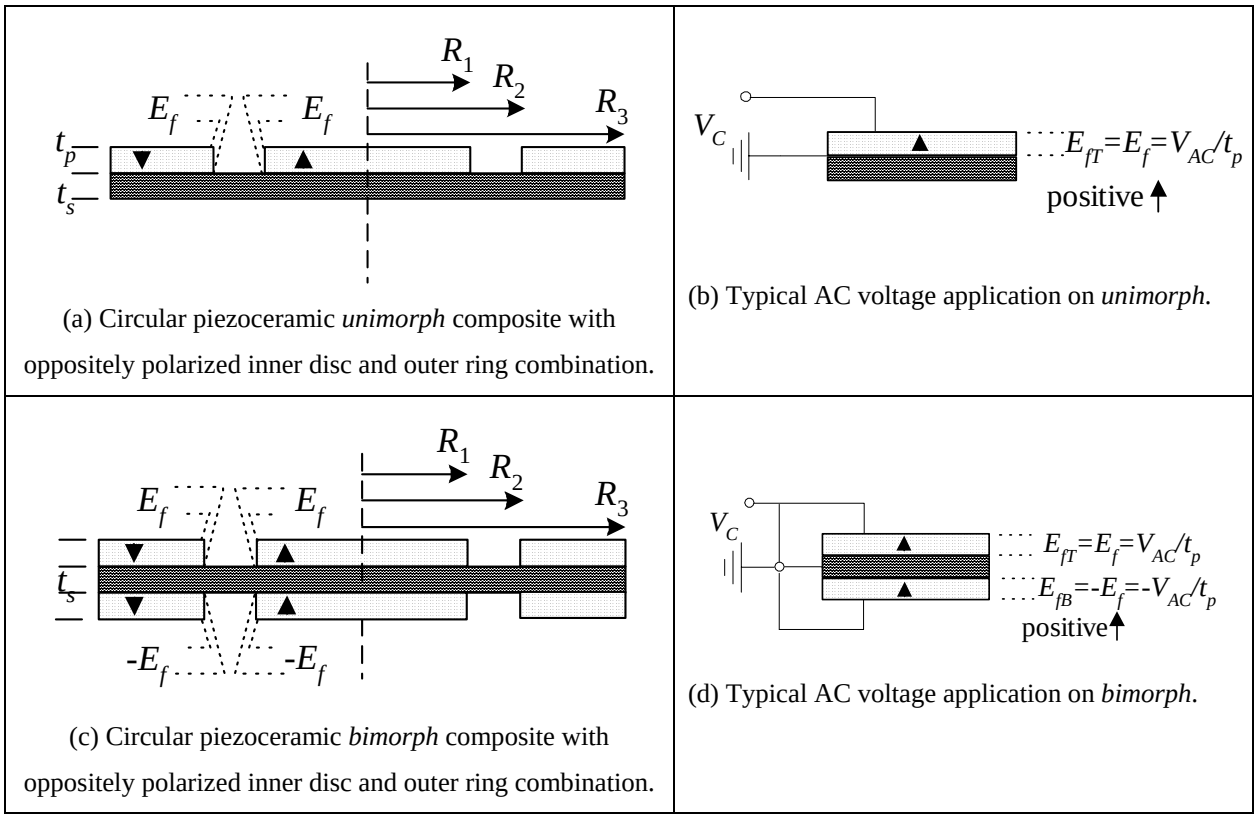

Figure 8 **: Circular composite piezoceramic plate configurations for synthetic jet optimization. Arrow tips represent the polarization direction and E_f denotes the positive upward electric field applied through a patch.**

- Compared to the Case I and II results (Table 2 and Table 3) reported in Gallas et al.,[11] an optimized *unimorph* configuration **increases the volume displacement by factors of 3 and 2.4**, respectively, for the same natural frequency and R_3 if no practical lower bound is applied for the shim and piezoceramic layer thickness. Similarly, an optimized *bimorph* configuration **increases the volume displacement by factors of 5.1 and 4.4**, respectively. This increase translates directly into increased velocity output of a synthetic jet.
- An optimum bimorph was designed to achieve a target volume displacement while simultaneously maximizing f_D with *estimated* lower constraints imposed on t_s and t_p due to manufacturing limitations, 3 and 5 mil, respectively. The

results, which are directly dependent on these constraints, are summarized in Table 5 below and indicate that a powerful piezoelectric synthetic jet with reasonable bandwidth can be achieved via optimization. Our model suggests f_D as much as 1660 Hz. which may be increased further if the thinner shim thickness can be manufactured.

Table 5: **Optimization results of bimorph composite with $Q = 430 \times 10^{-10} m^3$ and max(f_D) with several minimum gauge for t_s and 5 mil minimum gauge of t_p.**

Design	t_s 3 mil	t_s 1 mil	t_s 0.5 mil	t_s 0.3 mil	t_s 0.03 mil
R_3 *(mm)*	14.5	14.5	14.5	14.5	14.5
R_2 *(mm)*	14.5	14.5	14.5	14.5	14.5
R_1 *(mm)*	13.60	14.35	14.35	14.48	14.48
t_s *(mm)/(mil)*	0.0762 / 3	0.0254 / 1	0.0127/ 0.5	0.00762 / 0.3	0.002 / 0.08
t_p *(mm)/(mil)*	0.1434 / 5.6	0.228 / 8.9	0.2359 / 9.3	0.2447 / 9.6	0.2486 / 9.8
f_D *(Hz)*	1659	2180	2228	2278	2298
$Q\ x10^{-10}\ (m^3)$	430	430	430	430	430
V_{max} *(V)*	169	269	279	289	294

Conclusions

The optimization of piezoelectric-driven synthetic jet actuators based on LEM has been carried out. It has been shown that LEM is a viable tool to optimally design these devices for candidate applications. To simplify the problem, the current study has split the optimization problem into two parts by separately optimizing the (1) cavity volume and orifice dimensions and (2) the piezoelectric diaphragm. Significant enhancements in performance are obtained. A Matlab-based design optimization tool has been developed. Future work will add a graphical user interface to the Matlab code and will develop a corresponding user's guide.

Students Supported

Quentin Gallas

Damian Ricci

Dissertations

Gallas, Q., "On the Modeling and Design of Zero-Net Mass Flux Actuators," Ph.D. Dissertation, Department of Mechanical and Aerospace Engineering, University of Florida, Gainesville, FL, 2005.

Ricci, D., "Design of a Clamped Rectangular Composite Piezoelectric Diaphragm For Synthetic Jets," M.S. Dissertation, Department of Mechanical and Aerospace Engineering, University of Florida, Gainesville, FL, 2005.

Publications Resulting from this Work

Gallas, Q., Holman, R., Raju, R., Mittal, R., Sheplak, M., and Cattafesta, L., "Low Dimensional Modeling of Zero-Net Mass Flux Actuators," AIAA Paper 2004-2413, 2nd AIAA Flow Control Conference, Portland, OR, June 2004.

Gallas, Q., Holman, R., Sheplak, M., Mittal, R., and Cattafesta, L., "Modeling and Design of Zero-Net Mass Flux Actuators for Active Flow Control," *International Symposium on Recent Advances in Aeroacoustics and Active Flow-Combustion Control*," in Honor of Prof. John E. Ffowcs Williams, Goa, India, January, 2005. (invited)

Gallas, Q., Wang, G., Papila, M., Sheplak, M., and Cattafesta, L., "Optimization of Synthetic Jet Actuators," AIAA Paper 2003-0635, January 2003.

Gallas, Q., Mittal, R., Sheplak, M., and Cattafesta, L. "Case I - Lumped Element Modeling of a Zero-Net Mass Flux Actuator Issuing into a Quiescent Medium," *CFD Validation of Synthetic Jets and Turbulent Separation Control*, NASA Langley Research Center Workshop, Williamsburg, VA, March 29-31, 2004.

Gallas, Q., Mittal, R., Sheplak, M., and Cattafesta, L. "Case II - Lumped Element Modeling of a Zero-Net Mass Flux Actuator Interacting with a Grazing Boundary Layer," *CFD Validation of Synthetic Jets and Turbulent Separation Control*, NASA Langley Research Center Workshop, Williamsburg, VA, March 29-31, 2004.

Holman, R., Utturkar, Y., Mittal, R., Smith, B., and Cattafesta, L., "A Jet Formation Criterion for Synthetic Jets," in press, *AIAA Journal*, 2005.

Rupesh, K., Ravi, B., Mittal, R., Gallas, Q., and Cattafesta, L. "Time-Accurate Numerical Simulations of Synthetic Jets in Quiescent Air," *CFD Validation of Synthetic Jets and Turbulent Separation Control*, NASA Langley Research Center Workshop, Williamsburg, VA, March 29-31, 2004.

Utturkar, Y., Holman, R., Mittal, R., Carroll, B., Sheplak, M., and Cattafesta, L., "A Jet Formation Criterion for Synthetic Jet Actuators," AIAA Paper 2003-0636.

Utturkar, Y., Mittal, R., Rampunggoon, P., and Cattafesta, L., "Sensitivity of Synthetic Jets to the Design of Jet Cavity," AIAA Paper 2002-0124.

References

1. Cattafesta, L., Garg, S., and Shukla, D., "Development of Piezoelectric Actuators for Active Flow Control," *AIAA Journal*, Vol. 39, No. 8, pp. 1562-1568, August 2001.
2. Gallas, Q., Holman, R., Nishida, T., Carroll, B., Sheplak, M., and Cattafesta, L., "Lumped Element Modeling of Piezoelectric-Driven Synthetic Jet Actuators," *AIAA Journal*, Vol. 41, No 2, January 2003.
3. Gallas, Q., "On the Modeling and Design of Zero-Net Mass Flux Actuators," Ph.D. Dissertation, Department of Mechanical and Aerospace Engineering, University of Florida, Gainesville, FL, 2005.
4. Smith, B. L. and Glezer, A., "The Formation and Evolution of Synthetic Jets," Physics of Fluids, Vol. 10, No. 9, pp. 2281-2297, 1998.
5. Smith, B.L. and Glezer, A., "Vectoring and Small-Scale Motions Effected in Free Shear Flows Using Synthetic Jet Actuators," AIAA paper 97-0213, 1997.
6. Crook, A., Sadri, A. M., and Wood, N. J., "The Development and Implementation of Synthetic Jets for the Control of Separated Flow," AIAA Paper 99-3176, July 1999.
7. Amitay, M., Kibens, V., Parekh, D., and Glezer, A., "The Dynamics of Flow Reattachment Over a Thick Airfoil Controlled by Synthetic Jet Actuators," AIAA paper 99-1001, 1999.
8. Crook, A., Sadri, A. M., and Wood, N. J., "The Development and Implementation of Synthetic Jets for the Control of Separated Flow," AIAA Paper 99-3176, July 1999.
9. Rathnasingham, R. and Breuer, K. S., "Coupled Fluid-Structural Characteristics of Actuators for Flow Control," *AIAA Journal*, Vol. 35, No. 5, pp. 832-837, May 1997.
10. Lee, C.Y., and Goldstein, D.B., "DNS of Microjets for Turbulent Boundary Layer Control," AIAA paper 2001-1013, 2001.
11. Gallas, Q., Wang, G., Papila, M., Sheplak, M., and Cattafesta, L., "Optimization of Synthetic Jet Actuators," AIAA Paper 2003-0635, January 2003. (revision in preparation for submission to *AIAA J*)
12. Gallas, Q., Holman, R., Raju, R., Mittal, R., Sheplak, M., and Cattafesta, L., "Low Dimensional Modeling of Zero-Net Mass Flux Actuators," AIAA Paper 2004-2413, 2nd AIAA Flow Control Conference, Portland, OR, June 2004.

13. Gallas, Q., Holman, R., Sheplak, M., Mittal, R., and Cattafesta, L., "Modeling and Design of Zero-Net Mass Flux Actuators for Active Flow Control," *International Symposium on Recent Advances in Aeroacoustics and Active Flow-Combustion Control*," in Honor of Prof. John E. Ffowcs Williams, Goa, India, January, 2005. (invited)

14. Rossi, M., Acoustics and Electroacoustics, Artech House, Norwood, MA, pp. 245-373, 1988.

15. Mittal, R., Rampuggoon, P., Udaykumar, H. S., "Interaction of a Synthetic Jet with a Flat Plate Boundary Layer," AIAA Paper 2001-2773, June 2001.

16. Motsigner, R. E., and Kraft, R. E., "Design and Performance of Duct Acoustic Treatment," in Aeroacoustics of Flight Vehicles: Theory and Practice, Volume 2: Noise Control, edited by Hubbard, H. H., Acoustical Society of America, New York, 1995.

17. Gallas, Q., Mittal, R., Sheplak, M., and Cattafesta, L. "Case II - Lumped Element Modeling of a Zero-Net Mass Flux Actuator Interacting with a Grazing Boundary Layer," *CFD Validation of Synthetic Jets and Turbulent Separation Control*, NASA Langley Research Center Workshop, Williamsburg, VA, March 29-31, 2004.

18. Gallas, Q., Holman, R., Raju, R., Mittal, R., Sheplak, M., and Cattafesta, L., "Low Dimensional Modeling of Zero-Net Mass Flux Actuators," AIAA Paper 2004-2413, 2nd AIAA Flow Control Conference, Portland, OR, June 2004.

19. Prasad, S., Horowitz, S., Gallas, Q., Sankar, B., Cattafesta, L., and Sheplak, M., "Two-Port Electroacoustic Model of an Axisymmetric Piezoelectric Composite Plate," AIAA Paper 2002-1365, 43rd AIAA/ASME/ASCE/AHS Structures, Structural Dynamics, and Materials Conference, April 2002.